[PS]Predicting Fracability in Shale Reservoirs*

Milton Enderlin[1,2], Helge Alsleben[3], and John A. Breyer[1,3]

Search and Discovery Article #40783 (2011)
Posted July 31, 2011

*Adapted from poster presentation at AAPG Annual Convention and Exhibition, Houston, Texas, USA, April 10-13, 2011

[1]Energy Institute, Texas Christian University, Fort Worth, Texas (j.breyer@tcu.edu)
[2]Gearhart Company, Fort Worth, Texas
[3]School of Geology, Energy, and the Environment, Texas Christian University, Fort Worth, Texas

Abstract

Effectiveness of fracture stimulation techniques is controlled by the heterogeneous and anisotropic nature of rocks. Sedimentologic and stratigraphic models, the interaction of present-day and induced stress, and rock material properties, which are constrained by composition and mineral distribution, nature of primary sedimentary fabric, and presence and orientation of preexisting planes of weakness, can explain rock behavior.

The Barnett Shale in the Fort Worth basin is dominated by siliceous mudstone to claystone with a clay-mineral and cryptocrystalline quartz matrix. Laminated argillaceous lime mudstone and skeletal, argillaceous lime packstone are also abundant and several other facies are less common. Facies distributions in the central and eastern part of the basin are related to their location relative to advancing shale wedges and differ between proximal, distal, axial, and fringe depositional settings.

Fracability is a function of material brittleness and ductility, which can be inferred from Young's modulus and Poisson's ratio. We calculate values from bulk density and acoustic slowness well-log measurements and incorporate unconfined compressive strength (UCS) and internal friction angle (IFA) strength parameters with these constants. Hand-held penetrometer and micro-rebound hammer (MRH) measurements are used to estimate UCS and IFA. These measurements are performed at a frequency and scale as to be reconcilable with well logs and detailed petrographic, fabric and TOC data and allow calibration of petrographic data and indices of brittleness and ductility with log readings.

To address the behavior of shale reservoirs, we integrate qualitative and quantitative data. These data include core and thin section descriptions, penetrometer and MRH readings, description of present-day stress field, using a stress-strength equilibrium stress polygon approach, which includes estimates of overburden stress, maximum horizontal stress, minimum horizontal stress, and direction of maximum horizontal stress. Using stress estimates, fracture orientation data from borehole image logs, and pore pressure estimates, we calculate pressures needed to reactivate favorably oriented preexisting planes of weakness in shear. This approach establishes a means of calibrating lithology with well log response, allows correlation between lithology and rock strength, and predicts fracability based on these features and the nature of the in situ stress field.

Predicting Fracability In Shale Reservoirs

(Point Count to Production)

Milton Enderlin[1, 2], Helge Alsleben[3], John A. Breyer[1, 3]

[1]Energy Institute, Texas Christian University, Fort Worth, Texas, [2]Gearhart Company, Fort Worth, Texas, [3]School of Geology, Energy, and the Environment, Texas Christian University, Fort Worth, Texas

Abstract

Effectiveness of fracture stimulation techniques is controlled by the heterogeneous and anisotropic nature of rocks. Sedimentologic and stratigraphic models, the interaction of present-day and induced stress, and rock material properties, which are constrained by composition and mineral distribution, nature of primary sedimentary fabric, and presence and orientation of preexisting planes of weakness, can explain rock behavior.

The Barnett Shale in the Fort Worth basin is dominated by siliceous mudstone to claystone with a clay mineral and cryptocrystalline quartz matrix. Laminated argillaceous lime mudstone and skeletal, argillaceous lime packstone are also abundant and several other facies are less common. Facies distributions in the central and eastern part of the basin are related to their location relative to advancing shale wedges and differ between proximal, distal, axial, and fringe depositional settings.

Fracability is a function of material brittleness and ductility, which can be inferred from Young's modulus and Poisson's ratio. We calculate values from bulk density and acoustic slowness well log measurements and incorporate unconfined compressive strength (UCS) and internal friction angle (IFA) strength parameters with these constants. Hand-held penetrometer and micro-rebound hammer (MRH) measurements are used to estimate UCS and IFA. These measurements are performed at a frequency and scale as to be reconcilable with well logs and detailed petrographic, fabric and TOC data and allow calibration of petrographic data and indices of brittleness and ductility with log response.

To address the behavior of shale reservoirs, we integrate qualitative and quantitative data. These data include core and thin section descriptions, penetrometer and MRH readings, description of present-day stress field using a stress-gradient equilibrium stress polygon approach, which includes estimates of overburden stress, maximum horizontal stress, minimum horizontal stress, and direction of maximum horizontal stress. Using stress estimates, fracture orientation data from borehole image logs, and pore pressure estimates, we calculate pressures needed to reactivate favorably oriented preexisting planes of weakness in shear. This approach establishes a means of calibrating lithology with well log response, allows correlation between lithology and rock strength, and predicts fracability based on these features and the nature of the in situ stress field.

Supposition

We view fracability as the ease in which a rock can be forced into supporting a complex fracture network proximal to the wellbore. We define an index of fracability (fracability index = FI) that is equal to the average of the sum of the Brittleness Index (BI) and Stressed Fracture Index (SFI) so that FI = (Brittleness Index (BI) + Stress Fracture Index (SFI))/ 2.

Brittleness (B) is an important rock property. However, no universally accepted concept or measurement method exists (Altindag and Guney, 2010). Models used to quantify brittleness range from the slope of the stress-strain curve after the ultimate strength point has been reached (Jaeger and Cook, 1979) to ratios and combinations of hardness, fracture toughness, unconfined compressive strength (UCS), tensile strength, Young's modulus, and Poisson's ratio. For expediency, we have chosen to use the following methodologies and expressions to quantitative indices of brittleness.

1. Point Count:
   Jarvie's Brittleness = $B_J = (V_{SiO2}) / (V_{clay} + V_{SiO2} + V_{CaCO3})$
   Breyer's Brittleness = $B_B = \{(V_{SiO2}) / (V_{clay} + V_{SiO2} + V_{CaCO3} + V_{other})\}$ X SCM
   SCM = Strength Coefficient Multiplier
   V_{SiO2} = Volume quartz, V_{clay} = Volume clay,
   V_{CaCO3} = Volume Carbonate, V_{other} = Volume of other constituents
2. Micro-mechanical testing: From Rickman et al. (2008), referred to here as Mullen (M),
   B_M core = $\{[(E - 1)/7] + [(v - 0.4)/ - 0.25]\}/2$
   E = Young's Modulus (static)
   v = Poisson's Ratio
3. Petrophysical log analysis: From Rickman et al. (2008), referred to here as Mullen (M),
   B_M log = $\{[(E - 1)/7] + [(v - 0.4)/ - 0.25]\}/2$
   E = Young's Modulus (static)
   v = Poisson's Ratio

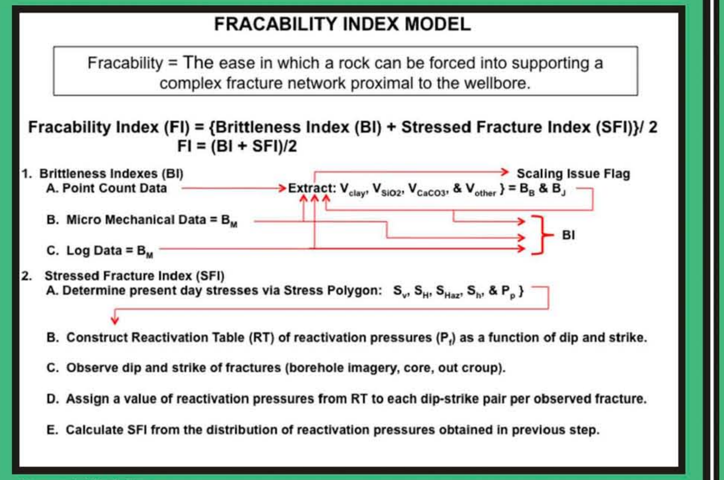

Figure 1. Work flow.

We also view the interaction of present-day stress with natural fractures and the ease of the fractures to be reactivated during hydrologic fracture stimulation, thereby producing seismic events on a very small scale (e.g. -3 magnitude), as an influential mechanism for the development of a complex fracture network proximal to the wellbore. The ease with which a particular orientation of fractures can be reactivated is quantified here as the stressed fracture index (SFI), which is a function of the fracture reactivation pressure (P_f), pore pressure (P_p), vertical stress (S_v), and net pressure (np). SFI is illustrated in Figure 28.

Setting / Introduction

- Shale-gas systems show significant differences in lithology and other reservoir properties within basins.
- Intrabasinal differences within continuous accumulations account for the indistinctly bound areas of better production termed "sweet spots" by operators.
- Several sets of facies have been recognized in the Barnett Shale in the Fort Worth basin (Breyer et al., 2011).
- Work in the central and eastern portion of the basin has related the geographic and stratigraphic distribution of facies within the Barnett to the location of the depositional site on depositional shale wedges (Monroe and Breyer, 2011). Facies in proximal areas of the wedges differ from facies in distal areas, and axial positions differ from facies deposited on the fringes of the wedges.

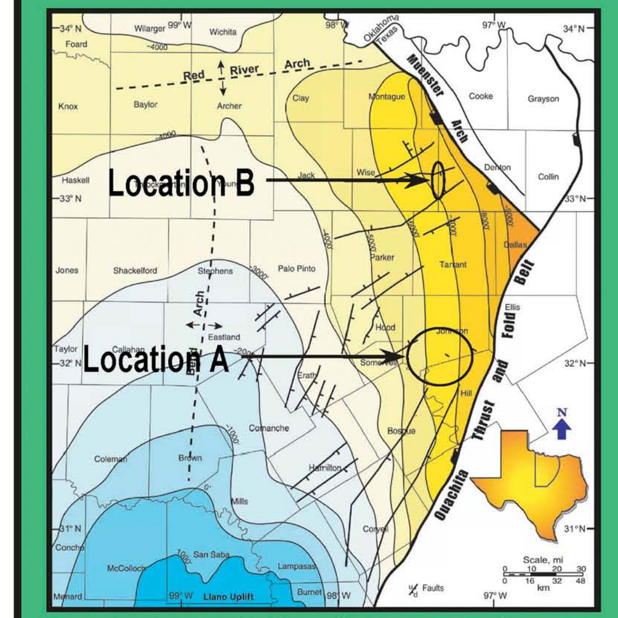

Figure 2. Location of well data. (Map modified from Zhao et al., 2007)

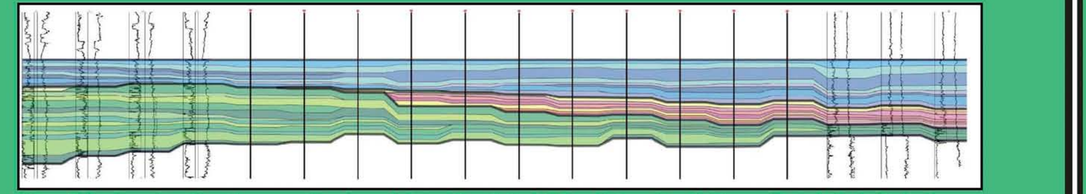

Figure 3. Northwest-southeast cross-section from Johnson County to Hill County (Location A). Green = Barnett Shale; Red colors = middle unit; Blue colors = upper unit. Due to proprietary data, several logs are not displayed in the cross-section (from Monroe, 2009).

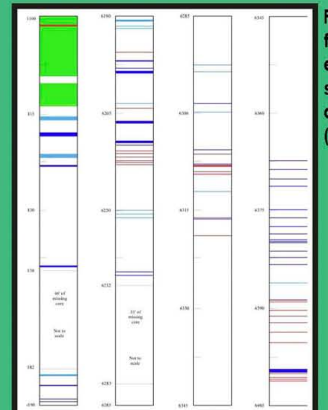

Figure 4. Bunting (2007) identified five facies that are distributed throughout the stratigraphic section of the Barnett Shale in core from west Johnson County (Location A).

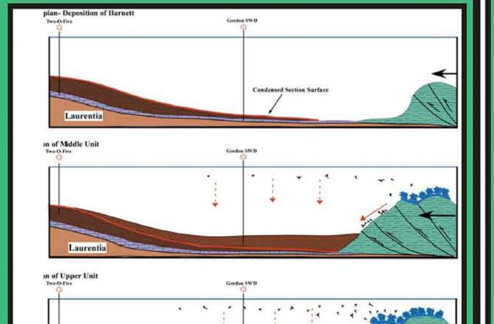

Figure 5. Interpretation of the depositional environment for the Barnett Shale, middle unit and upper unit in Hill County (from Monroe, 2009).

Barnett Shale: West Johnson County, Texas (Location A)

Brittleness Index (BI)

1. Point Count Data:

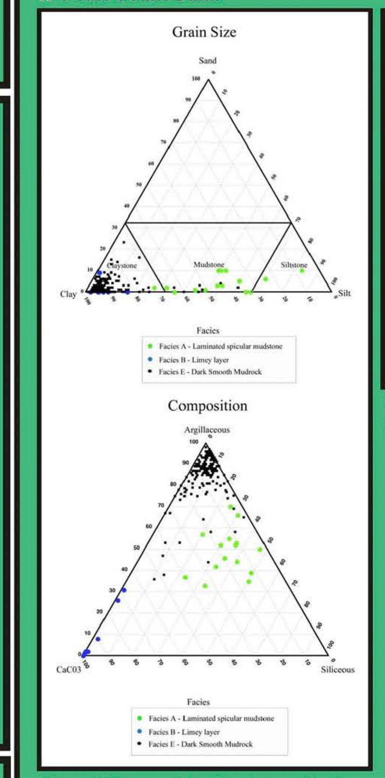

Figure 6. Ternary plots showing results of point count data from Location A (from Bunting, 2007).

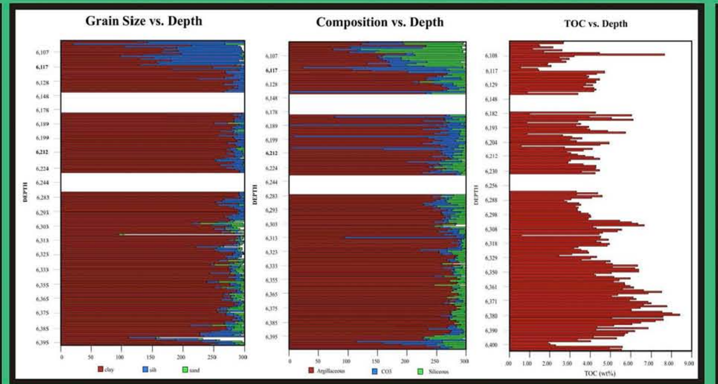

Figure 7. Variations in grain size, composition, and Total Organic Carbon (TOC) concentration with depth.

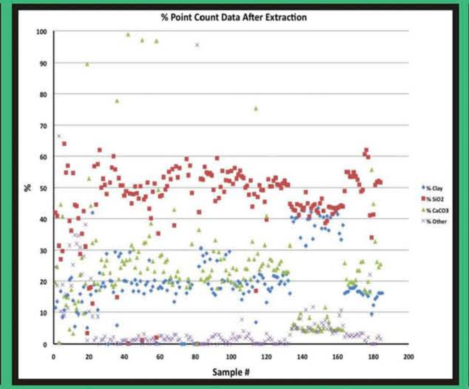

Figure 8. Point count data after "extraction" of volumes (see Figure 1).

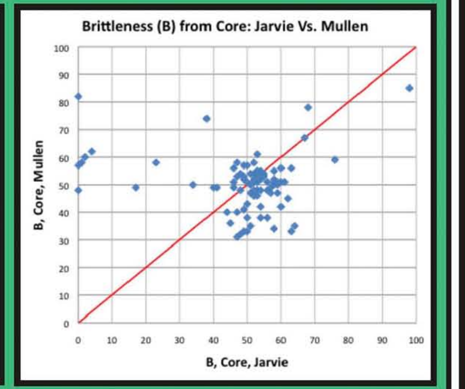

Figure 9. Plot of B_M vs. B_J.

Results of Core Analyses from NW Johnson County
- Dark, siliceous mudstone to claystone with a matrix of clay minerals and cryptocrystalline quartz is the most common facies in the Barnett Shale.
- Calcareous facies are the second-most abundant facies in the Barnett Shale
- With the exception of laminated spicular mudstone (Facies A on Figure 4) all samples generally have high clay concentrations (Figure 6).
- Concentrations of argillaceous materials are dominant (Figure 6).
- Concentrations of silt-sized particles and siliceous material are greatest near the top of the Barnett Shale (Figure 7).
- TOC concentrations increase toward the lower half of the core (Figure 7).

Figure 8 is the result of an extraction process that utilizes a form of Neural-Optic processing (Enderlin and Lenzer, 1994), which iterates between B_B and B_J with B_M core for the best match using B_M as a reference. A few samples had XRD analysis performed, and the results were used as initial reference points. Figure 9 shows the final results for the iteration between B_M and B_J, while Figure 10 displays the final results between B_M and B_B. When it was difficult to achieve a reasonable match between B_B and B_J with B_M core, a "scaling Issue" flag was issued (see Figure 1). The same philosophy was used regarding the match between B_M core and B_M log.

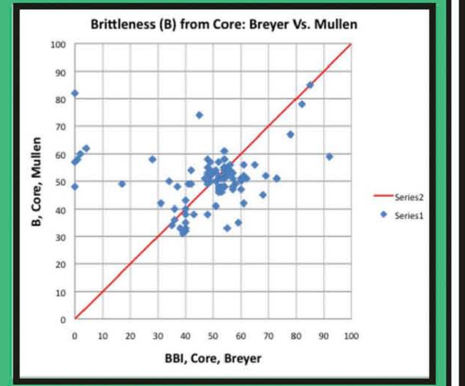

Figure 10. Plot of B_M vs. B_B.

2. Micro-Mechanical Testing:

Figure 11. Core photo of siliceous mudstone and calcareous facies (light colored), which are most abundant in the Barnett Shale.

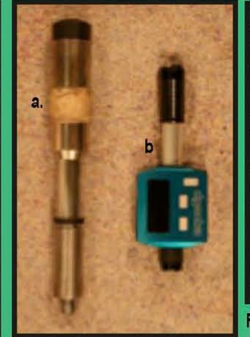

Figure 12. Hand-held micro-mechanical testing devices: a. Dimpler, b. micro rebound hammer (MRH).

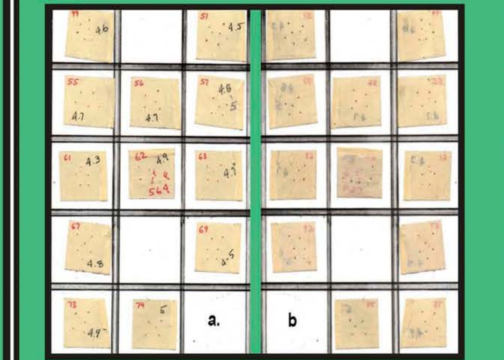

Figure 13. Dimple tapes on a clear plastic sheet: a. front, b. back.

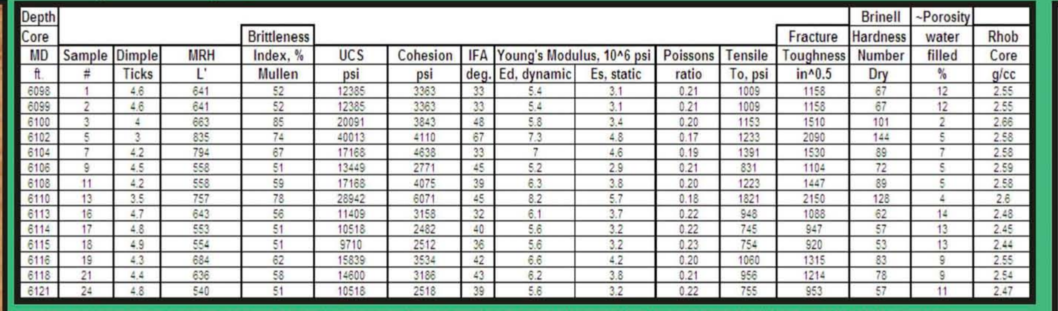

Figure 14. Results of a proprietary scheme for regressing non-unique correlations with dimple diameter "ticks" and MRH's L' values.

Micro-Mechanical Testing Procedure:
Figure 11 is a photograph of a typical section of core on which micro-mechanical testing was performed.
Dimpler: Compliant tape is placed on the core sample. The conical tip of the Dimpler (Figure 12a) indenter is coated with a (red) dye and then forced, at a constant axial load, through the tape and into the core sample creating a conical red marked depression (dimple) on the tape (Figure 13). (See Ramos et al. (2008) for operational concept of the Dimpler). The tape with dimple marks is removed and placed on clear plastic so that the front side and adhesive side of the tape are visible for analysis (Figure 13). A surface magnifier, scaled in ticks, is used to measure the Dimple diameters. Diameters are converted into an index of Unconfined Compressive Strength (UCS) (See Enderlin and Alsleben (in press) or Enderlin et al. (2010) for Dimpler response curve).
Micro Rebound Hammer (MRH): The MRH (Figure 12b) is placed upon the core sample and the impactor shuttle is activated. The velocity with which the impactor shuttle rebounds off the core surface is measured as an L' number. See Zahm and Enderlin (2010) for relationships of L' to UCS.

Analysis of Micro-Mechanical Testing:
Regressing with published correlations from Deere and Miller (1996), Weingarten and Perkins (1995), Rickman et al. (2008) and Gidley et al. (1989) with Dimpler derived UCS and MRH L' values yield non-unique solutions for the attributes found in Figure 14. Figures 15 and 16 show the relationship between core B_M and UCS with B_M and UCS from logs.

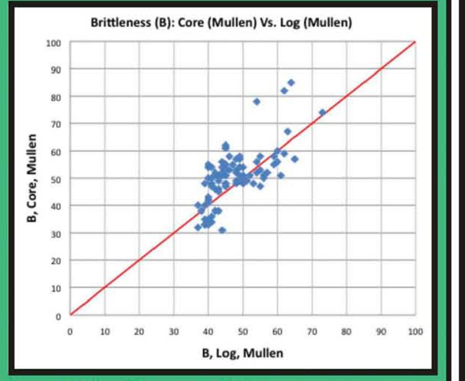

Figure 15. Plot of B_M core vs. B_M log.

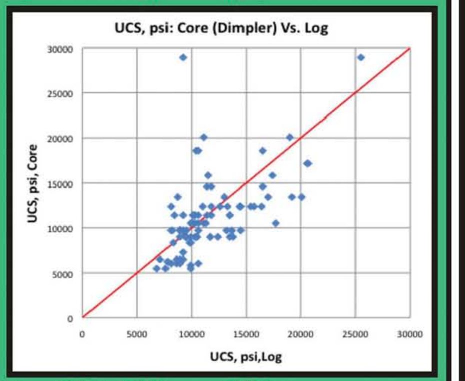

Figure 16. Plot of UCS core vs. UCS log.

3. Log Data:

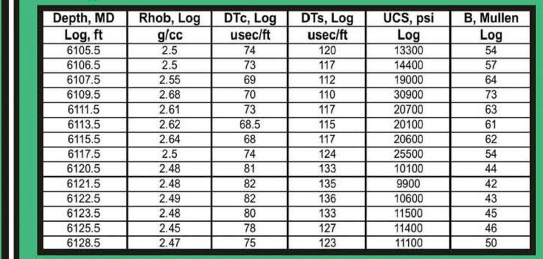

Figure 17. UCS and B_M from petrophysical log analyses.

In this case, the determination of rock strength from log measurements requires fluid substitution to account for the presence of overpressured gas and then project the log values to 100% water saturation (S_W = 100) at a normally pressured state. Once accomplished, strength evaluation was performed. Figure 17 displays a few feet of log input data and outputs of unconfined compressive strength (UCS) and B_M log. Figure 18 presents UCS from log, UCS from core along with their respective bulk density (Rho_b).

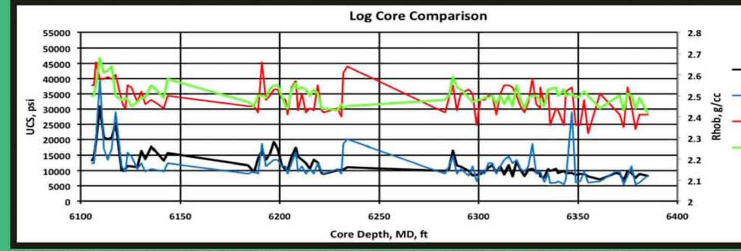

Figure 18. Comparison of UCS and Rho_b derived from micro-mechanical testing and log measurements.

4. Selecting Brittleness Index (BI):

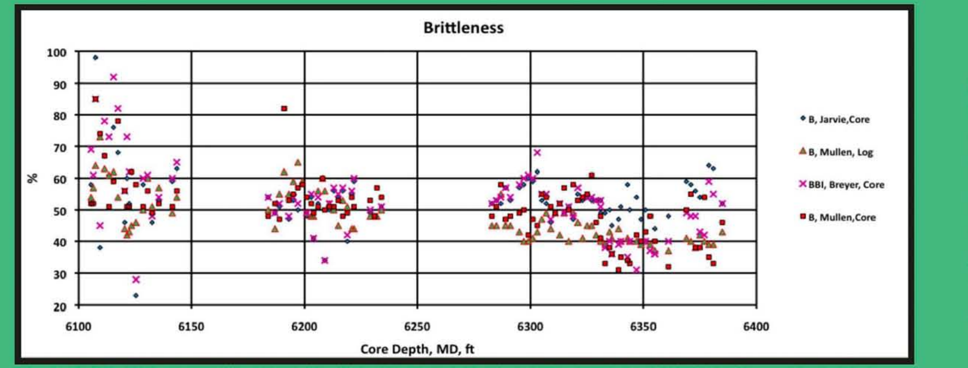

Figure 19. Comparison of brittleness (B_J, B_B, B_M) derived from point counting, micro-mechanical testing and log measurements. For the interval displayed, a BI of ~55% would be a reasonable value.

It is worth noting the spread of BI values at similar depth as a function of the measurement method's support volume. Micro-mechanical testing, thin section point counting, and logging provide insight into the complexity of the lithology and potential scaling issues (see Figure 1). For example, the interval between 6100 and 6125 ft contains considerable scatter whereas the section around 6200 ft is relative behaved. The upper section contains numerous strong phosphate nodules (see 6102 ft in Figure 19).

Stress Fracture Index (SFI)

1. Characterizing Present-Day Stress:

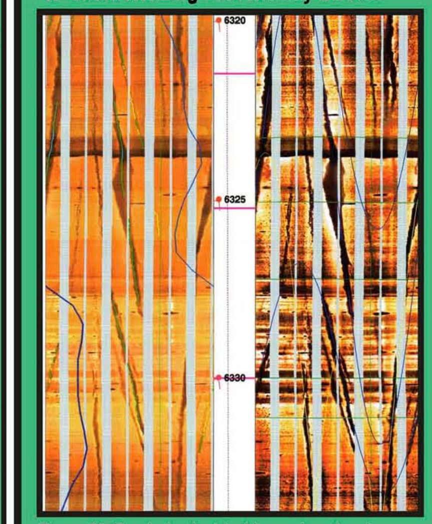

Figure 20. Borehole electrical image log showing drilling-induced tensile cracks.

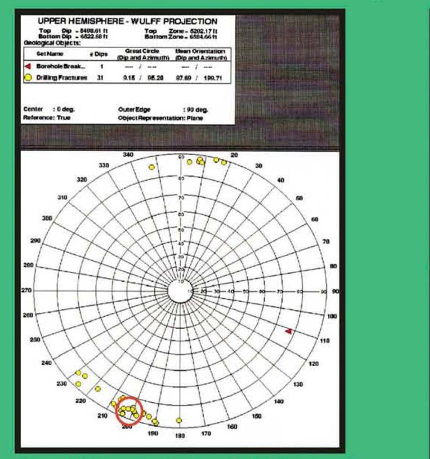

Figure 21. Upper hemisphere Wulff plot of poles to drilling-induced tensile cracks suggesting the maximum horizontal stress direction (SHaz) is ~115°.

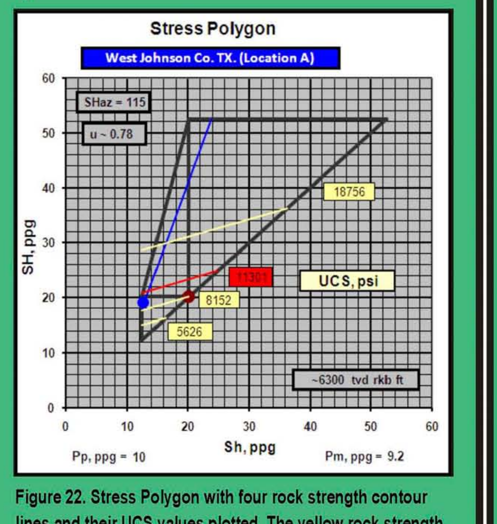

Figure 22. Stress Polygon with four rock strength contour lines and their UCS values plotted. The yellow rock strength lines are positioned for reference only. The red line and associated value box correspond to the estimated rock strength of interest (11300 psi). S_v is identified by the dark red dot and the blue dot marks the estimated present-day state of stress.

Using the methodology outlined in Zoback (2007) with the strength data from the previous section, borehole image information (Figure 20 and 21), particularly the presence of drilling-induced tensile cracks, pore pressure data, value for the coefficient of sliding friction (u) and mud weight information, the present-day stress state is graphically estimated via a stress polygon (Figure 22).

2. Determining Fracture Reactivation (Reactivation Table - RT):

Project the subsurface stresses (S_v, S_H, S_h) onto the surfaces of mechanical discontinuities, spatially defined by strike and dip, and resolve the normal and shear stresses. See Figure 23. Calculate, as a function of strike and dip, the fluid pressure required to make the product of the normal stress, less fluid pressure and u equal to the shear stress as described by Barton et al. (1995). Values are presented in Figure 24.

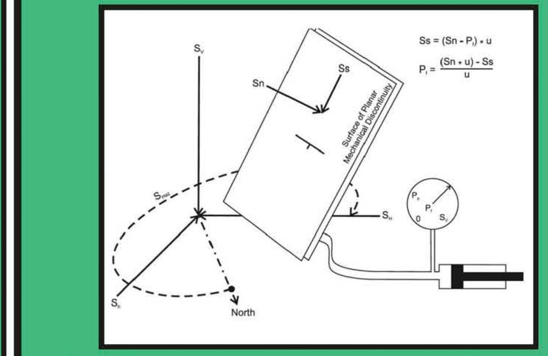

Figure 23. Arbitrary planar mechanical discontinuity surface spatially described by strike and dip is placed in a stress field described by S_v, S_H, S_h, and S_{Haz}. The normal stress (Sn) and shear stress (Ss) can be calculated. Reactivation occurs by increasing P_f such that the product of (Sn - Pf) and u is less than Ss.

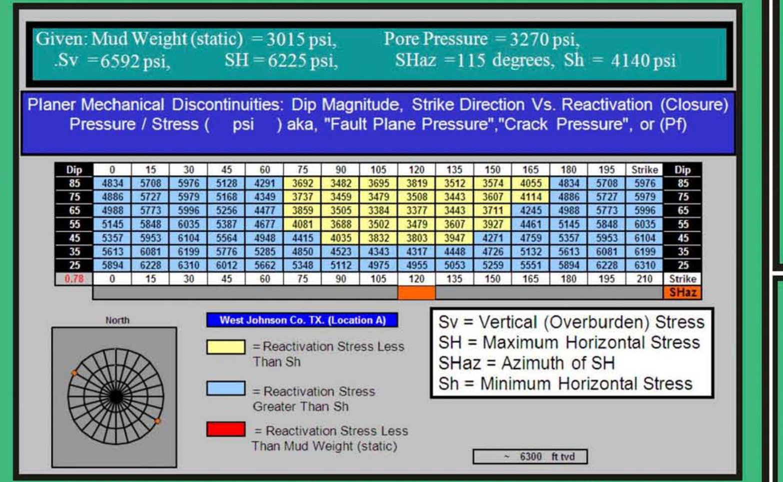

Figure 24. Plot of reactivation pressure (P_f) as a function of dip and strike [Reactivation Table (RT)]. The value in each cell represents the pressure (P_f in psi) required within a fault, fracture, crack, or bedding plane surface required to reactivate and fail in shear at the posted strike and dip values. Values assume constant coefficient of sliding friction (u) of 0.78 (posted in the lowermost left cell) and zero cohesion. Color code is as follows: Yellow: Required pressure for reactivation that is less than S_h; Blue: Reactivation at pressures that are greater than S_h; Red: Reactivation pressure less than mud pressure.

3. Observed Fractures:

Figure 24 displays the P_f for selected strike-dip pairs. The task is to find which pairs exist in the fracture data. The fracture data may be derived from field observations, core inspection, microseismic event locations, seismic studies, and petrophysical well logs. In all cases both strike and dip must be resolved. Here, the results of "poles to planes" are derived from the analysis of a borehole electric imager log and are plotted in Figures 25 and 26. The red arrows show the association between reactivation table and poles to planes.

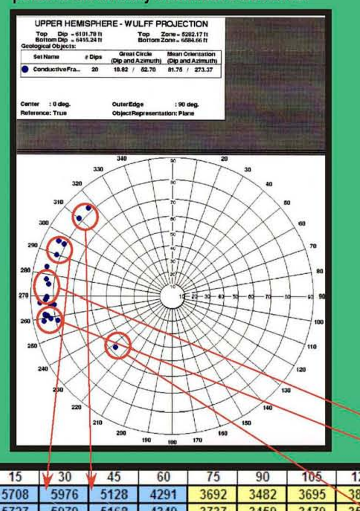

Figure 25. Upper hemisphere Wulff plot of poles to electrically conductive fractures.

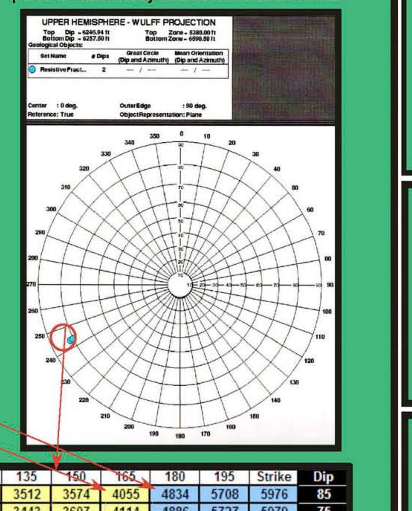

Figure 26. Upper hemisphere Wulff plot of poles to electrically non-conductive fractures.

4. Determining Stress Fracture Index (SFI):

The calculation of SFI differentiates observed fractures that are inconsequential, favorable and detrimental to the development of a complex fracture network proximal to the wellbore via hydraulic fracturing fluids. Inconsequential fractures are those with P_f less than the sum (A) of S_h and net-pressure, which, therefore, cannot be reactivated. Fractures, like faults, with a P_f close to P_p would easily reactivate, thereby diverting the fracturing fluid, and never allow the fracturing pressure to exceed the S_h to form Mode I fractures. Pressure B is the detrimental threshold pressure. Favorable fractures are those with P_f between A and B and normally reside near the interface on the yellow and blue cells on Figure 27.

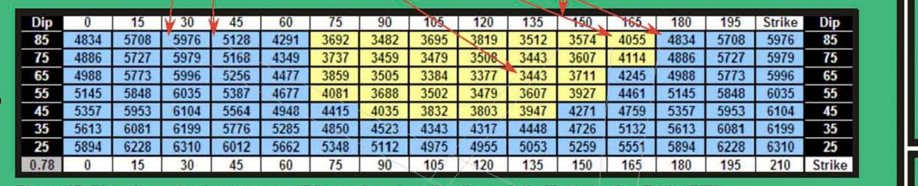

Figure 27. Plot of reactivation pressure (Pf) as a function of strike and dip [Reactivation Table (RT)].

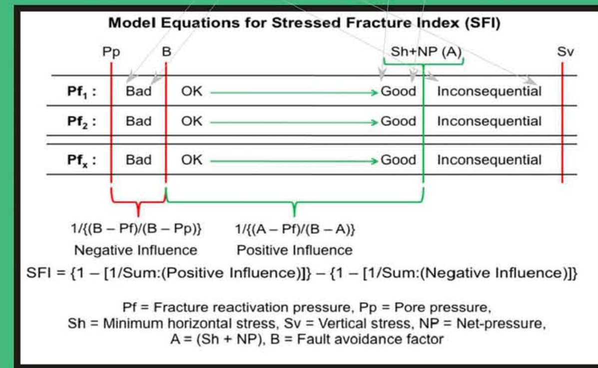

Figure 28. Expression for the calculation of the SFI. With B = 400 psi and NP = 800 psi, the SFI = 20%.

5. Determining Fracability Index (FI):

Using the value of SFI from Figure 28 and BI from Figure 19, the FI is calculated. FI = (BI + SFI) / 2 = (55% + 20%) / 2 = 38%

Barnett Shale: T.P. Sims #2, Denton-Wise County Line, Texas (Location B)

Brittleness Index (BI)

1. Micro-Mechanical Testing:

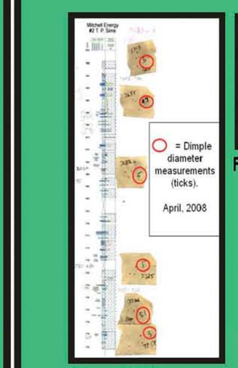

Figure 29. Micro-mechanical data.

Depth Core MD ft.	Dimple Ticks	MRH L'	Brittleness Index, % Mullen	UCS psi	Fracture Toughness in^0.5	Brinell Hardness Number Dry
7655	4.5	570	54	13449	1059	72
7682	5	596	48	8985	848	48
7725	5	560	46	8985	843	48
7734	5.1	580	47	8339	825	45

Figure 30. Results of micro-mechanical testing. Data in Figure 31.

Micro-mechanical data (Figure 29) was collected and analyzed with the results appearing in Figure 30. Petrophysical log analysis was conducted with the data available. Both the data and results are presented in Figure 31.

2. Log Data:

Depth, MD Log, ft	Rhob, Log g/cc	DTc, Log usec/ft	DTs, Log usec/ft	UCS, psi Log	B, Mullen Log
~ 7700	2.55	82	?	10500	46

Figure 31. UCS and B_M from petrophysical log analysis of data provided by Lancaster (1992).

3. Selecting Brittleness Index (BI): Data from core and logs suggest a BI value of ~ 46%.

Stress Fracture Index (SFI)

1. Characterizing Present-Day Stress:

Stress Polygon (Figure 32) was developed with the data from Lancaster (1992) to evaluate the present-day stresses. Reactivation table (Figure 33) was constructed from the stress information.

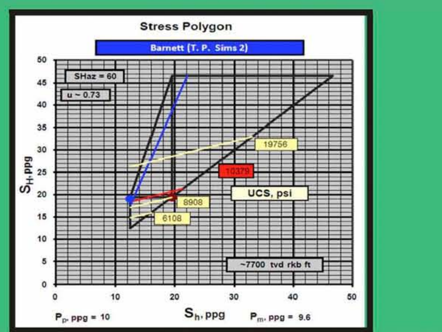

Figure 32. Stress Polygon

2. Determining Fracture Reactivation (Reactivation Table - RT):

Dip	0	15	30	45	60	75	90	105	120	135	150	165	180	195	Strike	Dip
85	5392	4480	4048	4200	4652	4200	4048	4480	5392	6548	7620	6548	5392	4480	4048	85
75	5468	4560	4076	4056	4188	4056	4076	4560	5468	6588	7596	6588	5468	4560	4076	75
65	5616	4732	4192	4000	3992	4000	4192	4732	5616	6668	7588	6668	5616	4732	4192	65
55	5836	5012	4444	4156	4080	4156	4444	5012	5836	6784	7592	6784	5836	5012	4444	55
45	6124	5396	4856	4544	4444	4544	4856	5396	6124	6932	7612	6932	6124	5396	4856	45
35	6464	5876	5420	5136	5040	5136	5420	5876	6464	7108	7640	7108	6464	5876	5420	35
25	6840	6416	6084	5872	5800	5872	6084	6416	6840	7296	7676	7296	6840	6416	6084	25
0.73	0	15	30	45	60	75	90	105	120	135	150	165	180	195	210	Strike

Figure 33. Reactivation Table

3. Observed Fractures:

Observed fractures (Figure 34) are projected on to the reactivation table (Figure 33) and the SFI and FI are calculated.

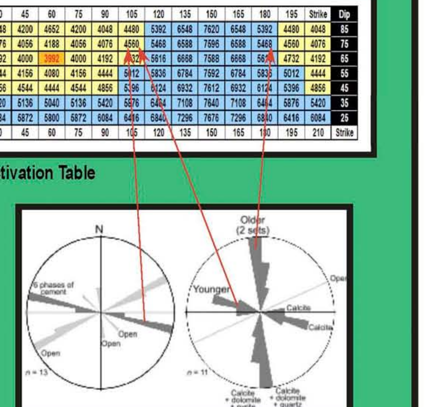

Figure 34. Fracture directions from Gale et al. (2007).

4. Determining Stress Fracture Index (SFI):
   With B = 400 psi, and NP = 800 psi, the SFI = 90%.

5. Determining Fracability Index (FI):
   FI = (BI + SFI) / 2 = (46% + 90%) / 2 = 68%

Production Reference (PR)

Production was evaluated by using data from the Texas Railroad Commission database particularly from the "Gas Well Back Pressure Test, Completion or Recompletion Report, and Log" Form G.

	Location A	Location B
API	n/a	49734514
Average of the highest first 3 months production (A3MP), MCF	24681	33164
Measured thickness of interval(MT), ft	3184	334
Production reference (PR) = A3MP / (product of MT, TVP, and NS), MCF / (MMgal ft NoS)	3.55	33.64

Stimulation:	Location A	Location B
Volume of acid, Kgal	0	0
Volume of water, Kbbl	53.8	34.99
Pounds of sand 1, MMlb	0.7285	0.1355
Pounds of sand 2, Klb	200	0
Total volume pumped (sand and water) (TVP), MMgal	2.311	1.476
Number of stages (NoS)	1	2

Fracability Index (FI) vs. Production Reference (PR)

	Location A	Location B
PR	3.55	33.64
FI	38%	68%

On the left is the comparison of Production Reference and Fracability Index, FI = (BI + SFI)/2, for the two locations. Whereas on the right is a comparison of Brittleness Index (BI) and Stress Fracture Index (SFI).

	Location A	Location B
BI	55%	46%
SFI	20%	90%

Implication

1. Once a fracture's P_f has been exceeded by pressure of the hydrologic fracturing fluids, shear failure occurs (activation). When pumping is stopped and the pressure of the hydrologic fracturing fluid falls below the P_f (deactivation), the "fall-off" pressure response, as a function of time, can be misconstrued as "closure" pressure (see Couzens-Schultz and Chan, 2010, also Mullen and Enderlin, 2010). Implying that traditional "closure" pressure value may or may not be equivalent to Sh.
2. Fractures with low P_f (center of the yellow sections of Figures 24, 27, and 33) need to be forced into a "tip-screen-out" condition in order to increase the bottom hole treating pressure to a value above Sh.

Conclusion

1. Fracability Index, as defined here, provides a numerical method for evaluating fracturing effectiveness by combining stratigraphic observations (particularly facies variations), rock properties (with emphasis on brittleness), natural fracture orientations (dip and strike), present-day stresses, pore pressure, and bottom hole hydrologic fracturing treating pressure.
2. The method presented also provides insights into the scaling issues regarding rock properties and stress distribution.

References

Altindag, R. and and Guney, A., 2010, Predicting the relationships between brittleness and mechanical properties (UCS, TS and SH) of rocks. Scientific Research and Essays Vol. 5(16), pp. 2107 - 2118, 18 August, 2010.
Barton, C.A., Zoback, M.D., and Moos. D., 1995, Fluid flow along potentially active faults in crystalline rocks: Geology, v. 23 p 683-686
Bunting, P.J., 2007, Petrographic analysis of the Barnett Shale in the Fort Worth Basin, (M.S. thesis), Texas Christian University, Fort Worth, TX, 111 p.
Couzens-Schultz, B.A. and Chan, A.W., 2010, An Alternative Leak-off Pressure Interpretation: Journal of Structure Geology, v. 6, no. 13
Deere, D.P., and Miller, R.P., Engineering Classification and Index Properties for Intact Rocks, Technical Report AFWL-TR-116, Air Force Weapons Laboratory, Kirtland , New Mexico, U.S.A. 327 p.
Enderlin, M., Weymer, B., D'Onfro, P., Ramos, R., Morgan, K. , 2010, The Unconfined Compressive Strength of SAFOD Core from Point-Load Penetrometer Tests. AAPG Annual Convention & Exhibition. 2010, April 13. New Orleans, Louisiana.
Enderlin, M. and Asleben, H., in press, A method for evaluating the effects of confining stress and rock strength on fluid flow along the surfaces of mechanical discontinuities in low permeability rocks, in Breyer, J.A. (ed.), AAPG Memoir 97 Shale Reservoirs—Giant Resources for the 21st Century, Tulsa, OK.
Enderlin, M. and Lenzer, D., 1994, Using strike resolved by neural-optic processing to determine dip in complex structures penetrated by deviated wells. AAPG annual convention. Annual Meeting Abstracts - AAPG and SEPM page 145.
Gale, J.F.W., Reed, R.M., and Holder, J., 2007, Natural fractures in the Barnett Shale and their importance for hydraulic fracture treatments: AAPG Bulletin, v. 91 no. 4, p. 603-622.
Gidley, J.L., Holditch, S.A., Nierode, D. E. and Veatch, R. W., 1989, Recent Advances in Hydraulic Fracturing, Monograph Vol. 12, SPE, Richardson, TX, 452 p.
Jaeger, J.C., and Cook, N.G., 1979, Fundamentals of rock mechanics, Chapman and Hall, New York, 585 p.
Lancaster, D.E., McKetta, S.F., Hill, R.E., Guidry, F.K., and Jochen, J.E., 1992, Reservoir evaluation, completion techniques, and recent results from Barnett Shale development in the Fort Worth Basin: SPE 24884.
Monroe, R.M., 2009, Petrographic and stratigraphic analysis of the Barnett Shale (Mississippian) in Hill County, Texas: Evidence for eustasy and tectonism, (M.S. thesis), Texas Christian University, Fort Worth, TX, 155 p.
Mullen, M., and Enderlin, M., 2010, Is that frac job really breaking new rock of just pumping down a pre-existion plane of weakness? - The integration of geomechanics and hydraulic-fracture diagnostic, 44th U.S. Rock Mechanics Symposium, Salt Lake City, UT.
Ramos, G.G., Chin, L.Y., Enderlin, M.B., 2008, Up-scaling of Rock Mechanical and Petrophysical Properties from Grain Scale to Log Scale by Point-Stress and Wedge Indentation Tests. 42nd U.S. Rock Mechanics Symposium, San Francisco, California. U.S.A.
Rickman, R., Mullen, M., Petre, E., Grieser, B., and Kundert, B., 2008, A Practical Use of Shale Petrophysics for Stimulation Design Optimization: All Shale Plays Are Not Clones of the Barnett Shale, SPE115258
Weingarten, J.S. and Perkins, T.K., 1995, Prediction of sand production in gas wells: methods and Gulf of Mexico case studies: SPE 24797.
Zahm, C.K., and Enderlin, M., 2010, Characterization of rock strength in Cretaceous strata along the Stuart City Trend, Texas: Gulf Coast Association of Geological Societies Transactions, v. 60, p. 693-702.
Zhao, H., Givens, N.B., Curtis, B., Thermal maturity of the Barnett Shale determined from well-log analysis: AAPG Bulletin, v. 91 no. 4, p. 535-549.
Zoback, M.D., 2007 Reservoir Geomechanics: Cambridge University Press, 449 p.

Acknowledgements

The authors would like to thank EOG Resources for providing the access to core used in the analysis and The Gearhart Companies for providing the resources needed to conduct this research.